Published December , 2005

ARTICLE

Quantitative Analysis of the Voltage-dependent Gating of Mouse Parotid ClC-2 Chloride Channel

Jose Antonio de Santiago,[1] Keith Nehrke,[2,3] and Jorge Arreola[1,3]

[1]Instituto de Física, Universidad Autonóma de San Luis Potosí, San Luis Potosí, SLP 78290, México
[2]Department of Medicine, [3]Department of Pharmacology and Physiology, and Center for Oral Biology, University of Rochester, Rochester, NY 14642

Various ClC-type voltage-gated chloride channel isoforms display a double barrel topology, and their gating mechanisms are thought to be similar. However, we demonstrate in this work that the nearly ubiquitous ClC-2 shows significant differences in gating when compared with ClC-0 and ClC-1. To delineate the gating of ClC-2 in quantitative terms, we have determined the voltage (V_m) and time dependence of the protopore (P_f) and common (P_s) gates that control the opening and closing of the double barrel. mClC-2 was cloned from mouse salivary glands, expressed in HEK 293 cells, and the resulting chloride currents (I_{Cl}) were measured using whole cell patch clamp. WT channels had I_{Cl} that showed inward rectification and biexponential time course. Time constants of fast and slow components were ~10-fold different at negative V_m and corresponded to P_f and P_s, respectively. P_f and P_s were ~1 at −200 mV, while at $V_m \geq 0$ mV, $P_f \sim 0$ and $P_s \sim 0.6$. Hence, P_f dominated open kinetics at moderately negative V_m, while at very negative V_m both gates contributed to gating. At $V_m \geq 0$ mV, mClC-2 closes by shutting off P_f. Three- and two-state models described the open-to-closed transitions of P_f and P_s, respectively. To test these models, we mutated conserved residues that had been previously shown to eliminate or alter P_f or P_s in other ClC channels. Based on the time and V_m dependence of the two gates in WT and mutant channels, we constructed a model to explain the gating of mClC-2. In this model the E213 residue contributes to P_f, the dominant regulator of gating, while the C258 residue alters the V_m dependence of P_f, probably by interacting with residue E213. These data provide a new perspective on ClC-2 gating, suggesting that the protopore gate contributes to both fast and slow gating and that gating relies strongly on the E213 residue.

INTRODUCTION

ClC-2 is a widely distributed chloride (Cl^-) channel that belongs to the ClC family of Cl^- channels (Thiemann et al., 1992; Jentsch et al., 2002). Plasma membrane ClC channels are homodimers with two independent protopores that are activated by voltage and H^+ and Cl^- ions (Hanke and Miller, 1983; Richard and Miller, 1990; Pusch et al., 1995; Chen and Miller, 1996; Jentsch et al., 2002; Pusch, 2004). At the heart of the gating mechanism of ClC channels is the presence of both fast and slow gating processes (Miller and White, 1984; Richard and Miller, 1990; Chen, 2005). The kinetics and V_m dependence of these processes are responsible for the overall kinetics of ClC Cl^- channels. A protopore gate that is responsible for the fast gating controls opening and closing of individual protopores. A common gate, responsible for slow gating, acts on both protopores simultaneously.

Although ClC-0, ClC-1, and ClC-2 share ~50–60% sequence identity, these channels retain very important functional differences. Unlike ClC-0 and ClC-1, ClC-2 is a strong inward rectifier (Thiemann et al., 1992; Park et al., 1998). At the macroscopic level, ClC-2 Cl^- current (I_{Cl}) shows slow activation kinetics and does not decay even with pulses >50 s (Arreola et al., 2002). The ClC-0 and ClC-1 open probability (P_0) is increased by increasing external $[Cl^-]$ ($[Cl^-]_e$) (Chen and Miller, 1996; Rychkov et al., 1996). In contrast, ClC-2 P_0 is slightly affected by $[Cl^-]_e$ (Niemeyer et al., 2003) but is enhanced by increasing internal $[Cl^-]$ (Haug et al., 2003; Niemeyer et al., 2003). Moreover, the pH sensitivity of ClC-2 is different; lowering external pH (pH_e) to ~6.5 results in enhancement of ClC-2 I_{Cl}, while further acidification results in inhibition (Arreola et al., 2002). Thus, the titration curve of ClC-2 has a bell shape. In contrast, ClC-0 and ClC-1 I_{Cl} are both enhanced at low pH_e (Hanke and Miller, 1983; Rychkov et al., 1996). Despite these significant differences, ClC-0/ClC-2 heterodimers show two conductance levels, suggesting formation of double barrel channels (Weinreich and Jentsch, 2001). In addition, the opening of homodimeric ClC-2 displays fast and slow components, suggesting the presence of protopore and common gates (Cid et al., 2000; Arreola et al., 2002). Additional evidence gathered from mutant guinea pig ClC-2 channels also supports this idea: mutating residue E217 into a V results in channels without fast gating while mutating residue

Correspondence to Jorge Arreola: Arreola@dec1.ifisica.uaslp.mx

Abbreviation used in this paper: ORF, open reading frame.

Published December , 2005

C256 into an S results in channels with altered slow and fast gating (Niemeyer et al., 2003; Zuniga et al., 2004).

Analysis of ClC-2 currents using a double exponential function indicated that at positive voltages the slow component increased while the fast component decreased (Niemeyer et al., 2003). However, it has been shown in ClC-1 that the V_m dependence of each component is not directly equivalent to the V_m dependence of the fast and slow gates (Fahlke et al., 1996; Accardi and Pusch, 2000). Furthermore, although these two gates are determinant for the activity of ClC channels, the V_m dependence of a particular gate varies between channels. For example, macroscopic ClC-0 and ClC-1 I_{Cl} are quite similar. At first glance, one might think that the two gates have similar V_m dependence. But, at positive voltages, P_0 for the common gate decreases in ClC-0 while in ClC-1 increases. In contrast, P_0 for the protopore gate increases in both channels as V_m becomes positive (Lin et al., 1999; Accardi and Pusch, 2000). Thus, the relative weight of the fast and slow components obtained from a double exponential fit is not identical to the V_m dependence of the ClC-2 gates. This information cannot be inferred from the V_m dependence of the ClC-0 and ClC-1 gates, either. As a result, quantitative information about the protopore and common gates is needed in order to understand the gating behavior of ClC-2.

In this work, we sought to determine the V_m and time dependence of both the protopore and common gates underlying the V_m dependence of ClC-2 from mouse salivary glands (mClC-2). mClC-2 was expressed in HEK 293 cells and assessed using whole cell patch clamp. We found that P_0 of fast and slow gating decreased at positive V_m and that the corresponding time constants were about one order of magnitude different. In addition, we introduced point mutations in critical residues that are known to form part of the protopore and common gates in other ClC channels, including ClC-2 cloned from guinea pig (Lin et al., 1999; Accardi et al., 2001; Dutzler et al., 2003; Zuniga et al., 2004). The E213A mutation resulted in channels lacking the protopore gate. In addition to lacking fast gating, a significant influence on slow gating was observed in E213A mutant channels. In contrast, the C258S mutation failed to alter the slow gate but instead changed the V_m dependence of the protopore gate. Based on our results, we conclude that E213 is part of the protopore gate responsible for fast gating and partially responsible for the slow gating process. Residue C258 appears to be coupled to the protopore gate since the C258S mutation was redundant in an E213A background. These data are described using a double pore model with protopore and common gates. A preliminary report has been presented in abstract form (de Santiago and Arreola, 2005).

MATERIALS AND METHODS

ClC-2 Cloning and Site-directed Mutagenesis

The entire mouse ClC-2 open reading frame (ORF) including nucleotide −6 to 2727 relative to the start codon was amplified from mouse parotid gland (Nehrke et al., 2002) first strand cDNA using primers tagged with either EcoRI (at the 5′ end) or SalI (at the 3′ end). The ORF was then cloned into complementary sites in the vector pIRES2EGFP (CLONTECH Laboratories Inc.) to create the pIRES2EGFP-mClC2 construct. The clone was bidirectionally sequenced in full. A V685A alteration does not affect activity and is present in both the WT and mutant clones. Mutations were introduced using a Quikchange protocol (Stratagene) where complementary primers containing the mutation of interest were used with the vector template to produce PCR-amplified product. DpnI digestion was used to selectively degrade the template before transformation and clonal selection. For each mutation introduced, the ORF was again sequenced to ensure the absence of second-site mutations.

Cell Culture and Transient Transfection

HEK 293 cells obtained from Invitrogen were maintained at 37°C in a 95% O_2/5% CO_2 atmosphere. Cells for transient transfection were grown onto 30-mm Petri dishes to a 50–60% confluence. HEK 293 cells were transfected with the vector pIRES2EGFP-mClC2 (0.5 μg/μl) using Polyfect transfection reagent (QIAGEN) according to the manufacturer's instructions. Transfected cells were detached using trypsin and replated onto 5-mm diameter glass coverslips, then allowed to attach to the glass for 6 h before use.

Recording Solutions

External and internal solutions with symmetrical [Cl^-] and pH were used. External solution contained (in mM) TEA-Cl 139, $CaCl_2$ 0.5, 100 mM D-mannitol, and HEPES 20. The standard internal solution contained (in mM) TEA-Cl 140, EGTA 20, and HEPES 20. The pH in both solutions was adjusted to 7.3 with TEA-OH. The presence of D-mannitol made the external solution hypertonic compared with internal solution ($\Delta\Pi$ = 70 mosm/kg) to avoid activation of the volume-sensitive chloride channel present in these cells. The tonicity was determined using the freezing point method (VAPRO Wescor).

Electrophysiological Recordings

Coverslips with attached cells were placed into a recording chamber (~300 μl volume) mounted on the stage of an inverted microscope equipped with UV illumination. Cells were washed with the external media and observed under UV light to find fluorescent cells, since GFP fluorescence was used as reporter of successful transfection. Whole cell I_{Cl} was recorded using an Axopatch 200B and the pClamp 6 or 9 software (Axon Instruments, Inc.). Fluorescent cells were patched (Hamill et al., 1981) using electrodes fabricated with Corning 8161 glass (Warner Instrument Corp.) to have a resistance of 2.0–4.0 MΩ when filled with the internal solution. The recording chamber was grounded using a 3 M KCl agar bridge. I_{Cl} was recorded from +100 to −200 mV in 20-mV steps (unless otherwise is indicated) using voltage clamp steps delivered every 6 s from a holding potential of 0 mV. Currents were filtered at 5 kHz using a built-in 8 db/decade Bessel filter and then sampled at 10 kHz. Offline analysis was done using Clampfit (Axon Instruments, Inc.) and Origin packages. All experiments were performed at an ambient temperature of 21–23°C.

Analysis

Only whole cell currents with a reversal potential near 0 were included in our analysis. The currents were tested using a protocol that consisted of a hyperpolarization to −100 mV followed by a

Published December , 2005

ramp between −50 and +50 mV to measure variations in the reversal potential. Since the variations induced by hyperpolarization may indicate changes in $[Cl^-]$, we did not include in the analysis currents with reversal potentials different from zero. I-V curves were constructed using averaged relative I_{Cl}. Individual I-Vs were normalized to the current amplitude recorded at −200 mV. The apparent open probability (apparent P_o) was estimated from the instantaneous tail currents recorded at +60 mV as follows. Initial currents at +60 mV were plotted as a function of the test pulses and then fit with a Boltzmann function (Eq. 1) to estimate I_{max}.

$$P = P_{min} + \frac{P_{max} - P_{min}}{1 + e^{-\frac{zF}{RT}(V_m - V_{0.5})}}, \quad (1)$$

where P_{max} and P_{min} are maximum and minimum tail currents, respectively, z is the apparent gating charge, F the Faraday constant, R the gas constant, T the temperature, and $V_{0.5}$ is the V_m needed to reach $(P_{max} - P_{min})/2$. I_{max} values were used to normalize tail current data to obtain apparent P_0. The apparent P_0 data were then fit with Eq. 1. In that case, P_{max} (=1) and P_{min} represent maximum and minimum P_0 values.

Time constants were calculated by fitting I_{Cl} traces with a first order biexponential function:

$$I_{Cl}(t) = y_1(1 - e^{-t/\tau f}) + y_2(1 - e^{-t/\tau s}) + y_0, \quad (2)$$

where τ_f and τ_s are fast and slow time constants, respectively. $A_f = y_1/(y_0 + y_1 + y_2)$, $A_s = y_2/(y_0 + y_1 + y_2)$, and $C = y_0/(y_0 + y_1 + y_2)$ represent the relative contributions of fast, slow, and instantaneous components to the biexponential function. Time constants at positive voltages were obtained by fitting Eq. 2 to tail currents generated by first hyperpolarizing to −100 mV and then depolarizing at different voltages.

A method similar to the one used by Pusch et al. (2001) to analyze the effects of 2-(*p*-chlorophenoxy) butyric acid on ClC-0 was used here to model the protopore and common gates. Time constants and P_0 data were fed into the model to determine the rate constants. Differences between data and model predictions were minimized using the software Matematica 4 as exemplified below for the protopore gate model (Scheme 2). This model is characterized by two time constants and an open probability:

$$\chi = \sum_{V_m=80}^{V_m=-200} \frac{(\tau_{1m} - \tau_f)^2}{\sigma^2_f} + \sum_{V_m=80}^{V_m=-140} \frac{(\tau_{2m} - \tau_s)^2}{\sigma^2_s} + \sum_{V_m=80}^{V_m=-200} \frac{(P_m - P_f)^2}{\sigma^2_{Pf}} \quad (3)$$

where τ_{1m}, τ_{2m}, and P_m are time constants and apparent P_0 predicted by the model; τ_f, τ_s, σ_f, and σ_s are time constants and their experimentally determined SEM (Fig. 1 D); and P_f and σ_{pf} are the protopore gate P_0 and its experimentally determined SEM (Fig. 2 B). To determine the rate constants of the common gate (λ and μ) we performed a similar procedure using P_s and time constants shown in Fig. 4 (filled symbols). Current simulations were performed using a homemade program written in FORTRAN and Visual Basic (http://www.ifisica.uaslp.mx/~jadsc/ichsim.htm). Assumptions used in the model are described in RESULTS.

Data were analyzed without correction for leak or capacitative currents. Mean ± SEM are given or plotted and the number of experiments is indicated by *n*.

RESULTS

Voltage-dependent Properties of WT mClC-2

I_{Cl} recorded from HEK 293 cells transiently transfected with WT mClC-2 cDNA shows a characteristic inward rectification and slow time course of activation. Fig. 1 A depicts a family of I_{Cl} recorded between +60 and −130 mV. Resistance determined between +20 and +80 mV was 3812 ± 932 MΩ (n = 11). This is equivalent to ∼+26 pA at +100 mV, a value similar to that determined from untransfected cells and was considered leak current. I_{Cl} amplitude started from zero, indicating that the channels were closed at the holding voltage of 0 mV. I_{Cl} amplitude then slowly increased at negative V_m and reached steady state by the end of the 700-ms pulse. Channels closed quickly when the membrane was repolarized to +60 mV. The corresponding I-V curve is depicted in Fig. 1 B. Current amplitudes at each potential were normalized to the I_{Cl} value recorded at −200 mV and then pooled. Relative I_{Cl} was virtually zero at positive V_m but increased steadily as V_m was made negative. This behavior was due to a near zero apparent P_0 at positive V_m and an enhanced apparent P_0 at negative V_m (Fig. 1 C). From fitting the data with a Boltzmann function, it was estimated that channels reached half maximum activation at −94 ± 2 mV with an apparent gating charge of −0.75.

The onset kinetics of I_{Cl} displayed fast and slow components. Currents were fit with a double exponential function plus an instantaneous component (Eq. 2) to obtain the corresponding fast (τ_f) and slow (τ_s) time constants as well as the relative contribution of each component (A_f, A_s, and C). These time constants and the relative components are plotted as a function of V_m in Fig. 1, D and E, respectively. τ_f was ∼10 times smaller than τ_s at all V_m and both increased at positive V_m. Components A_f and A_s showed an opposite voltage dependence, A_f decreased at positive V_m and A_s increased. However, both components reached a maximum around 0 mV and crossed over around −150 mV. C component remained at ∼0 when $V_m < -50$ mV while it reached 0.12 ± 0.01 at −20 mV.

Voltage Dependence of the ClC-2 Gates

In a double barrel pore controlled by protopore and common gates, ion conduction occurs when the two gates are open. Fig. 1 (D and E) shows that for mClC-2, the I_{Cl} "on" kinetic is dominated by the fast component. This can happen if the slowest (common) gate is partially open and the faster (protopore) gate switches from closed to open. In addition, Fig. 1 C shows that the apparent P_0 decreased to zero at positive V_m. This can take place when P_0 of the protopore gate (P_f) goes back to approximately zero, assuming that P_0 of the common gate (P_s) is >0. Alternative possibilities (P_s = 0 and $P_f > 0$ or $P_s = 0$ and $P_f = 0$) predict slow kinetics, however, we show the presence of a rapid activation. Thus, it seems reasonable to assume that P_0 for the common gate would be >0 at positive V_m. An estimation of P_s at positive V_m can be computed assuming that

Published December , 2005

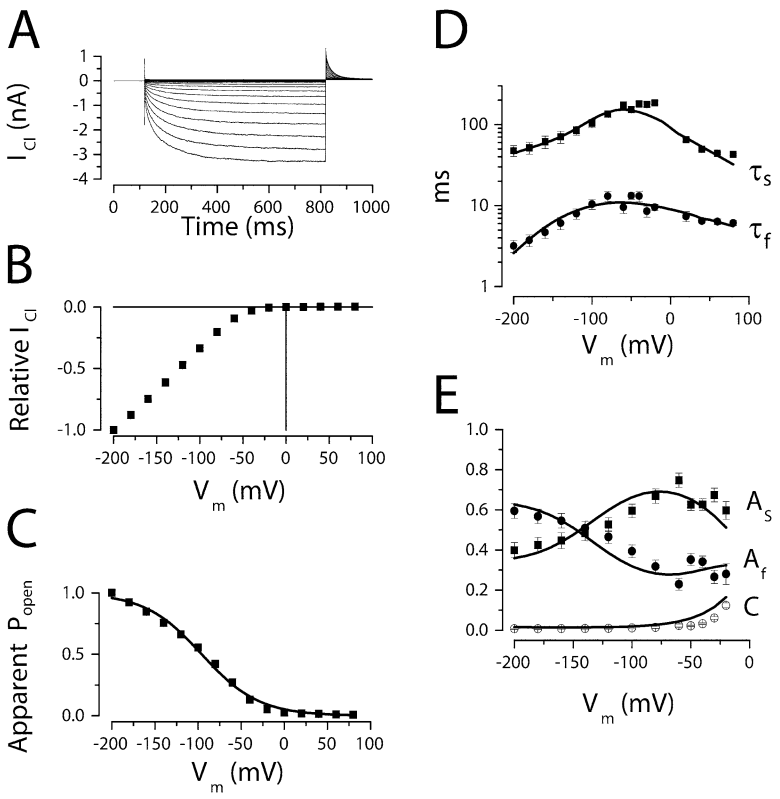

Figure 1. WT mClC-2 channels expressed in HEK 293 cells. (A) Raw traces elicited by voltage steps between +60 and −130 mV given in 10-mV increments. (B) I-V relationship (n = 9). I_{Cl} at each V_m was normalized to the corresponding value obtained at −200 mV and the resulting relative currents were averaged and plotted. (C) Apparent P_0 at each test pulse was estimated as the magnitude of the tail current recorded at +60 mV divided by I_{max} estimated from a Boltzmann fit (see description in MATERIALS AND METHODS; n = 7). Continuous line is the fit of Eq. 1. (D) Fast (τ_f) and slow (τ_s) time constants as function of V_m. Time constants were obtained by fitting raw data with Eq. 2. (E) Relative weight of fast, slow, and instantaneous components. D and E show that our model displayed in Fig. 6 was also able to account for the double exponential behavior of whole cell currents. Simulated currents, like those depicted in Fig. 7 B, were fit with Eq. 2 to determine τ_f, τ_s, A_f, A_s, and C. Those are plotted as continuous lines in D and E.

the two gates switch between one open and one closed state, with a fast time constant much faster than the slow time constant and $P_f = 0$. Under these conditions, I_{Cl} will be given by (Bennetts et al., 2001)

$$I_{Cl}(t) = 2Ni[P_{S\infty}P_{f\infty} - P_{S0}(P_{f\infty} - P_{f0})e^{-t/\tau f} - P_{f\infty}(P_{S\infty} - P_{S0})e^{-t/\tau s}], \quad (4)$$

where N is the number of channels; i is the single channel current; τ_f and τ_s are time constants for protopore and common gates, respectively; P_{s0} and $P_{s\infty}$ are the common gate P_0 at t = 0 and t = ∞, respectively; and P_{f0} and $P_{f\infty}$ are the protopore gate P_0 at t = 0 and t = ∞, respectively. It can be seen from Eq. 4 that I_{Cl} would increase rapidly if the common gate is partially open at the holding potential, that is $P_{s0} > 0$. Eq. 4 is similar to Eq. 2, with $A_f = P_{s0}/P_{s\infty}$ and $A_s = 1 - P_{s0}/P_{s\infty}$. Since at −200 mV, apparent P_0 is saturated (Fig. 1), this hints that both P_s and P_f have reached their maximum values, $P_{s\infty} = 1$ and $P_{f\infty} = 1$, respectively. Therefore, the common gate P_0 at the beginning of the −200 mV step would be $P_{s0} \approx A_f \approx 0.6$ (see Fig. 1 E). These computations indicate that the common gate must be partially open at positive V_m and that the gating of mClC-2 is compatible with the double barrel model controlled by two protopore gates and one common gate whose transitions follow Scheme 1.

To further test these ideas, the V_m dependence of mClC-2 channel gates was directly determined. To do so, a protocol similar to that used for hClC-1 was used (Accardi and Pusch, 2000). The protocol consisted in hyperpolarizing V_m to a desired test value for 500 ms followed by a 15-ms interpulse to −200 mV and back to the test voltage. Fig. 2 A shows a current trace using this protocol for a test voltage of −100 mV. The test pulse allowed both gates to reach steady-state P_0 values. The steady-state I_{Cl} at the end of the test voltage is given by $I_{Cl1} = 2NiP_sP_f$.

The interpulse to −200 mV quickly changed P_f to ∼1. Assuming that this interpulse did not disturb the common gate, the initial current upon returning to the test V_m must be proportional to P_s and is given by $I_{Cl2} = 2NiP_s$.

Thus, P_f at the test V_m was determined as I_{Cl1}/I_{Cl2}. Since this computation was done using I_{Cl} amplitude before and after the 15-ms interpulse, it has the advantage of correcting for any intracellular Cl^- depletion that might have occurred during the test pulse. This method was repeated for other test voltages to determine P_f as a function of V_m. The resulting graph is shown in Fig. 2 B (■). The protopore gate is fully open at very negative voltages, 50% open at −63 mV, and completely closed at voltages positive to zero. An apparent gating charge of −1.22 was estimated from fit with Eq. 1. P_s was determined by dividing the apparent P_0 (Fig. 1 C) by P_f and is shown as closed circles in Fig. 2 B. Unlike the protopore gate, the common gate did not close, remaining ∼55% open at positive V_m, completely

Published December , 2005

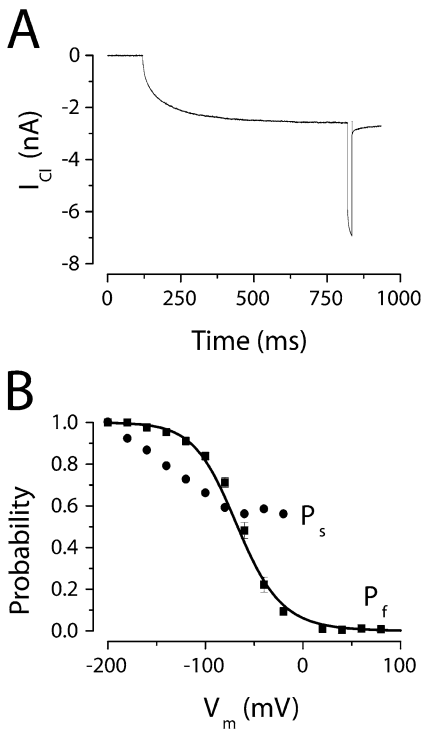

Figure 2. V_m dependence of WT mClC-2 protopore and common gates. (A) Raw current trace elicited by a voltage protocol that consisted of a test pulse to −100 mV followed by a 15-ms interpulse to −200 mV and then return to −100 mV. (B) Probability of P_f (■) or P_s (●) as a function of V_m. P_f was obtained as described in the text. P_s was obtained by dividing the values shown in Fig. 1 C by P_f. Continuous line was generated using Scheme 2.

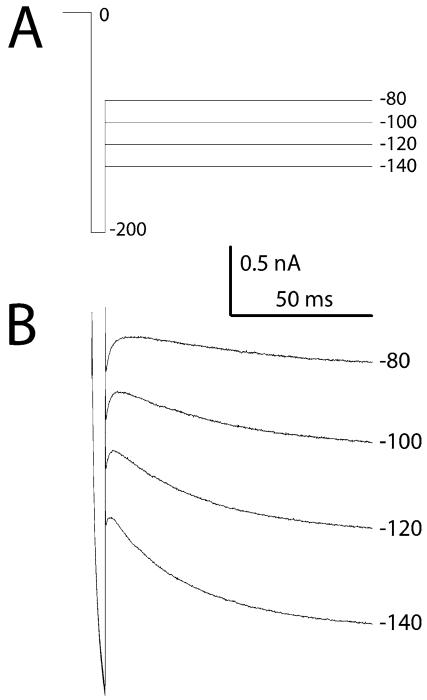

Figure 3. Two gates are present in mClC-2. (A) Voltage protocol. (B) I_{Cl} elicited by protocol shown in A. Note a transient decrease followed by a slow increase in current amplitude during the second variable step.

open at negative V_m, and half open at −134 mV with an apparent charge of −0.99. This result is entirely consistent with the predictions based on Fig. 1 E as described above.

Further support for the presence of protopore and common gates was collected from experiments in which cells were hyperpolarized to −200 mV during 5 ms and then repolarized to different voltages (Fig. 3 A). The duration of the first pulse was short and very negative to approach $P_f \sim 1$ without dramatically altering P_s. Upon repolarization to a less negative V_m (−140, −120, −100, or −80 mV), the contribution of P_f decreased from ∼1 to an intermediate value. In contrast, at those V_m the contribution of P_s increased until a steady-state value was reached. When the potential is repolarized, I_{Cl} is expected to first decrease and then increase. Fig. 3 B illustrates this phenomenon at the indicated voltages. By these criteria, mClC-2 expressed in HEK 293 cells displays a behavior that is compatible with the presence of both protopore and common gates.

As previously mentioned, ClC-0 and ClC-1 gating has been described using a six-state model (Pusch, 2004; Chen 2005). Nonconductive states had common and/or protopores gates in the closed state. Conductive states had the common gate and at least one protopore gate in the open state. The behavior of the two gates was best described by Scheme 1:

$$C_0 \underset{\gamma}{\overset{\delta}{\leftrightarrow}} C_1 \qquad \text{(SCHEME 1)}$$

where C_0 and C_1 are closed and open states, respectively, and transitions between states are controlled by V_m-dependent rate constants δ and γ. This model predicts an I_{Cl} with a biexponential behavior due to the presence of two gates (Eq. 4). In agreement with this model, mClC-2 I_{Cl} followed a biexponential time course. However, disagreement between mClC-2 data and the model arises when we compare experimental to predicted A_f and A_s values, taking into account the V_m dependence of P_f and P_s (see Fig. 2). The model did not reproduce A_f and A_s values shown in Fig. 1 E, instead predicted that at positive voltages the A_f and A_s parameters would increase and decrease, respectively (not depicted). This discrepancy suggests that a quantitative description of mClC-2 gating requires a modification of the model used to explain ClC-0 and ClC-1 behavior.

Our data show the presence of two gates in mClC-2, but indicate that a simple six-state model cannot explain these data. Discrepancies between the data and

Published December , 2005

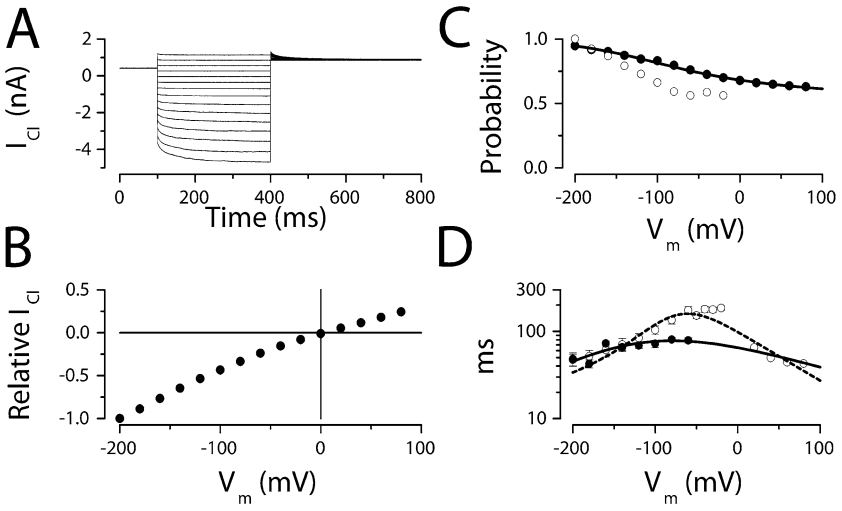

Figure 4. mClC-2 channels lacking the protopore gate (E213A mutant). (A) Macroscopic I_{Cl} generated by E213A mutant channels in the voltage range of +80 to −200 mV. Notice that at $V_m \geq -50$ mV, currents are time independent. (B) Normalized I-V curve for mutant E213A channels ($n = 7$). (C) Apparent P_0 in E213A mutant channels as a function of V_m ($n = 7$). Tail currents at +60 mV like those shown in A were used to estimate apparent P_0 values. For comparison purposes, P_s data from WT channels (Fig. 2 B) are shown as open circles. (D) Time constants for whole cell currents ($n = 7$) resulting from E213A mutant channel activation at the indicated V_m. For comparison, WT τ_s from Fig. 1 is plotted again as open circles and dotted line. Continuous lines in C and D are fits using Scheme 1.

the model could be due to the gates behaving differently from Scheme 1. To test this idea, each gate was studied separately to extract their contribution to the overall kinetics.

In torpedo ClC-0, hClC-1, and guinea pig ClC-2, the protopore gate is formed in part by a glutamic acid residue facing the conduction pathway near the external side of the channel (Dutzler et al., 2003; Estevez et al., 2003; Niemeyer et al., 2003). Thus, we sought to gain further insights into the V_m dependence of protopore and common gates of mClC-2 by removing this residue. The equivalent glutamic acid (E213) of mClC-2 was mutated into an alanine residue. The resulting I_{Cl} were time independent at voltages >-80 mV (Fig. 4 A). At very negative V_m, I_{Cl} showed an instantaneous current followed by a time-dependent component that exhibited a monoexponential behavior. The resulting normalized I-V curve was nearly linear (Fig. 4 B), indicating that the rectification is somehow associated with residue E213. The apparent P_0 vs. V_m relation of the mutant channels (Fig. 4 C, ●), estimated from the tail current at +60 mV, was shallow. At positive V_m, ~60% of channels were in the open state. Although there were some significant differences between WT and E213A channels, at very negative V_m, the time-dependent component of mutant E213A channel current was compatible with the slow gating component of WT mClC-2. Fig. 4 C compares E213A P_0 (●) to WT P_s (○). The apparent P_0 of the E213A shows the same trend as WT P_s. E213A apparent P_0 values were fit to a Boltzmann function with parameter of $V_{0.5} = -86$ mV and apparent charge $= -0.4$. In addition, time constants obtained by a single exponential fit to E213A I_{Cl} at negative V_m (Fig. 4 D, ●) were also quite similar to WT τ_s determined in Fig. 1 (Fig. 4 D, ○). Continuous lines in Fig. 4 (C and D) are fit to Scheme 1. Thus, in analogy with ClC-0 where the fast gating is due to the protopore gate and the slow gating is due to the common gate, we concluded that the slow time-dependent component of I_{Cl} obtained from mutant E213A reflects the voltage dependence of the common gate. Mutation E213A removed most of the fast gating and affected the slow gating at a relative less negative V_m (>-60 mV) values.

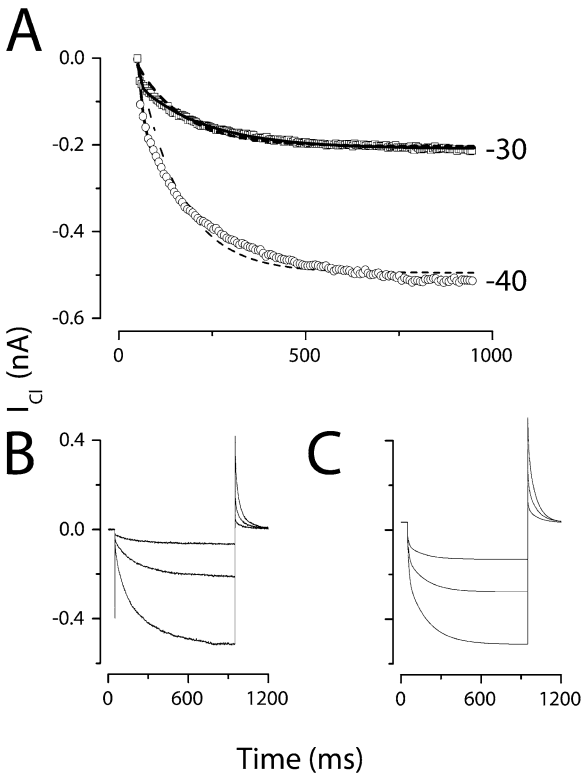

Figure 5. The protopore gate of WT mClC-2 exhibits biexponential behavior. (A) I_{Cl} recorded at −30 (■) and −40 (●) mV. Broken lines are single exponential fits and continuous lines are fits using a biexponential function. (B) I_{Cl} recorded at −20, −30, and −40 mV. (C) I_{Cl} was reproduced by using Scheme 2 and the membrane voltages indicated for B.

Published December , 2005

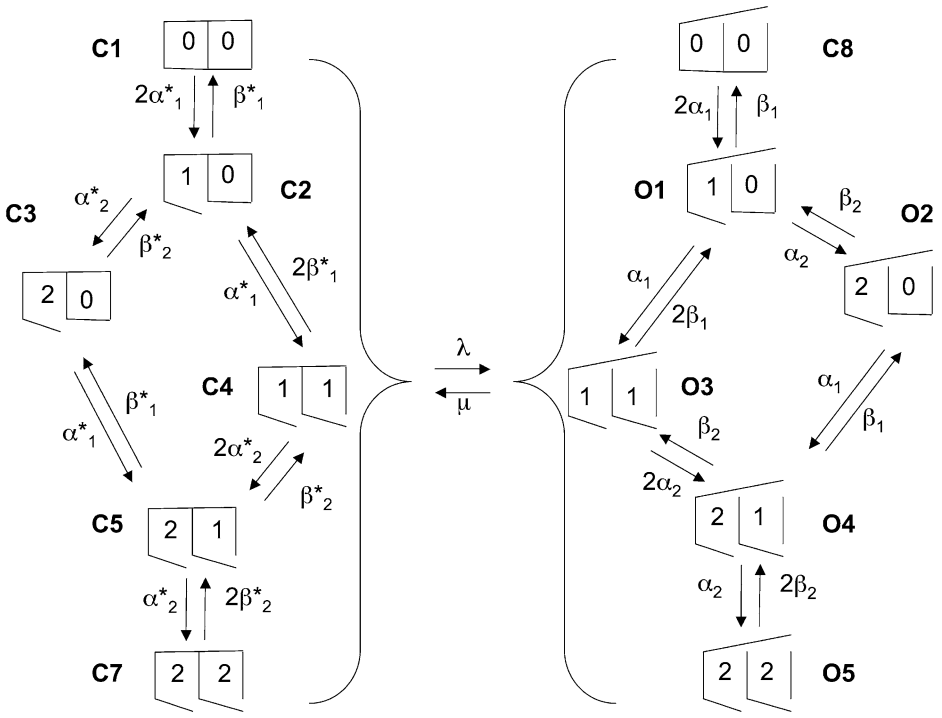

Figure 6. Kinetic model for mClC-2. A kinetic model developed to explain ClC-0 and ClC-1 was modified to account for the three states of the protopore gate. Scheme 1 describes the common gate. This resulted in a 12-state model consisting of seven nonconductive (C1–C7) and five conductive (O1–O5) states. Left column: states representing the common gate closed. Right column: states representing the common gate in the open position. Transitions between states are controlled by the indicated rate constants, these were assumed to be exponentially related to V_m. Transitions leading to the opening of the common gate (left column to right column) were assumed to follow the same kinetics and to be controlled by rate constants λ and μ. Likewise, we assumed that transitions of the protopore gate were independent of the common gate state. Free parameters were α_1, β_1, α_2, β_2, λ, and μ (see Table I).

Previous data show that the open to closed transitions for the mClC-2 common gate are described by Scheme 1. It was unclear whether or not the same description could be applied to protopore gate transition(s). To determine a plausible scheme to describe the protopore gate, we analyzed the time course of I_{Cl} recorded at $V_m > -50$ mV, where the common gate shows none or little V_m dependence (see Fig. 2 and traces in Fig. 4) and the activation kinetics must be due to the opening of the protopore gate alone. If Scheme 1 is used to describe the protopore gate kinetics, then I_{Cl} should follow a monoexponential time course. However, the time course for I_{Cl} recorded between −50 and 0 mV was not always monoexponential. Fig. 5 A shows that a biexponential function (continuous line) fits I_{Cl} better at −30 and −40 mV than a monoexponential function (broken line). Thus, Scheme 1 cannot explain the behavior of the protopore gate, and instead the data are compatible with a three-state scheme:

$$C_0 \underset{\beta_1}{\overset{\alpha_1}{\leftrightarrow}} C_1 \underset{\beta_2}{\overset{\alpha_2}{\leftrightarrow}} C_2 \qquad \text{(SCHEME 2)}$$

where C_0, C_1, and C_2 are one closed and two open states for the protopore gate, respectively, and α_1, α_2, β_1, and β_2 are the rate constants. In Fig. 5 (B and C), the recorded data are compared with currents simulated using Scheme 2. As can be seen, the general properties of the data can be simulated with Scheme 2. Thus, kinetics of WT ClC-2 currents have three components, one from slow gating and two from fast gating. Two components were readily observed while the third component was apparent only when currents are analyzed at $V_m > -50$ mV.

Quantitative Description of mClC-2 Function

Opening and closing of ClC channels is determined jointly by the V_m dependence and the transitions of their protopore and common gates. The V_m dependence of the two components is shown in Fig. 2 B and Fig. 4 C and their expected kinetics described by Schemes 1 and 2. In this section we propose a plausible kinetic model for mClC-2. For simplicity the Cl^- and pH dependencies were not included. Fig. 6 shows a 12-state model. 0, 1, and 2 denotes the three states of the protopore gate according to Scheme 2. The left column shows six nonconductive states that include the common gate in the closed position and different conformations for the protopore gate. The column to the right shows states that incorporate an open common gate with a protopore gate in every viable position. Of the states shown, only those labeled O1 through O5 are conductive. In a general case, transitions between states were considered independent and controlled by a respective rate constant. Unfortunately, this case leads to large number of free parameters that made the model excessively complicated for routine use. To simplify it, we assumed that regardless of the protopore gate the transitions of the common gate remained unchanged and were controlled by the on rate constant λ and the backward rate constant μ. Similarly, we assumed that transitions of the protopore gate were autonomous from the common gate state. These assumptions re-

Published December , 2005

TABLE I

Rate Constants Derived from Fits to ClC-2 Data Using the 12-State Model

Model rate constants: $\varepsilon = \varepsilon_0 \exp^{zVF/RT}$ (s^{-1})				
ε	ε_0	Z		
α_1	4.1	−0.57		
β_1	100.3	0.18		
α_2	6.4	−0.2		
β_2	10.6	0.32		
λ	1.7	−0.30	8.8	0.14
μ	4.9	0.18		

P_f or P_s data along with the corresponding time constants were used to estimate V_m-dependent rate constants after a minimization procedure. The functions used to extract the rate constants at different voltages were obtained by solving (Matematica 4) the differential equations representing Schemes 1 (common gate) and 2 (protopore gate). P_m and τm (model open probability and time constant) for Scheme 1 are given by $P_m = \lambda/(\lambda + \mu)$ and $\tau_m = 1/(\lambda + \mu)$. P_m, $\tau 1m$, and $\tau 2m$ (model open probability and time constants) for Scheme 2 are given by $P_m = \alpha_1(\alpha_2 + \beta_2)/[(\beta_1\beta_2 + \alpha_1(\alpha_2 + \beta_2)]$,

$$\tau_{1m} = 2/\left\{\alpha_1 + \alpha_2 + \beta_1 + \beta_2 + \sqrt{(\alpha_1 + \alpha_2 + \beta_1 + \beta_2)^2 - 4[\beta_1\beta_2 + \alpha_1(\alpha_2 + \beta_2)]}\right\},$$

and

$$\tau_{2m} = 2/\left\{\alpha_1 + \alpha_2 + \beta_1 + \beta_2 - \sqrt{(\alpha_1 + \alpha_2 + \beta_1 + \beta_2)^2 - 4[\beta_1\beta_2 + \alpha_1(\alpha_2 + \beta_2)]}\right\}.$$

Rate constants were assumed to be exponentially related to voltage as $\varepsilon_0 \exp^{zVF/RT}$ where ε_0 is the rate constant value at zero voltage, z is the apparent charge, V is the voltage, F is the Faraday constant, R the gas constant, and T the temperature.

duced to six (α_1, β_1, α_2, β_2, λ, and μ) the number of free parameters. Rate constants were assumed to be dependent on V_m in an exponential manner.

The rate constants α_1, β_1, α_2, and β_2 were extracted by simultaneously fitting Scheme 2 to experimentally determined P_f, τ_f, and τ_s shown in Fig. 2 B (■) and Fig. 1 D, respectively. Similarly, λ and μ were obtained by simultaneously fitting Scheme 1 to P_s and the time constants shown in Fig. 4, C and D (●), respectively. The time constants and P_0 for each gate that resulted from the model were minimized against the experimental data as described in MATERIALS AND METHODS. Table I shows the resulting rate constants that best fit the data.

To assess if the model was capable to reproduce the properties of mClC-2, we compared currents recorded from WT mClC-2 (Fig. 7 A) and model-based currents (Fig. 7 B) in a wide range of voltages (from +80 to −200 mV). Currents were simulated using a homemade program and the rate constants listed in Table I. The overall kinetics as well as the inward rectification of simulated currents were similar to those of WT ClC-2. The experimental apparent P_0 was also reproduced quite well (Fig. 7 C). In addition, Fig. 1 (D and E) shows that the model (continuous lines) describes well time constants and the relative contribution of A_f and A_s. The model can readily explain the properties of mutant E213A channels when P_f is removed. Fig. 7 (D and E) shows original recordings and currents simulated by the model lacking the protopore gate, respectively. Fig. 7 F shows that the apparent P_0 of the E213A mutant, obtained from data similar to that shown in Fig. 4 C and Fig. 7 D (filled symbols), can be predicted by the model (continuous line).

Are ClC-2 Gates Coupled?

Mutating C256 to serine in rat ClC-2 alters properties associated with the common gate such as Cd^{2+} and temperature sensitivities (Zuniga et al., 2004). Noteworthy is the observation that C256S channels closed

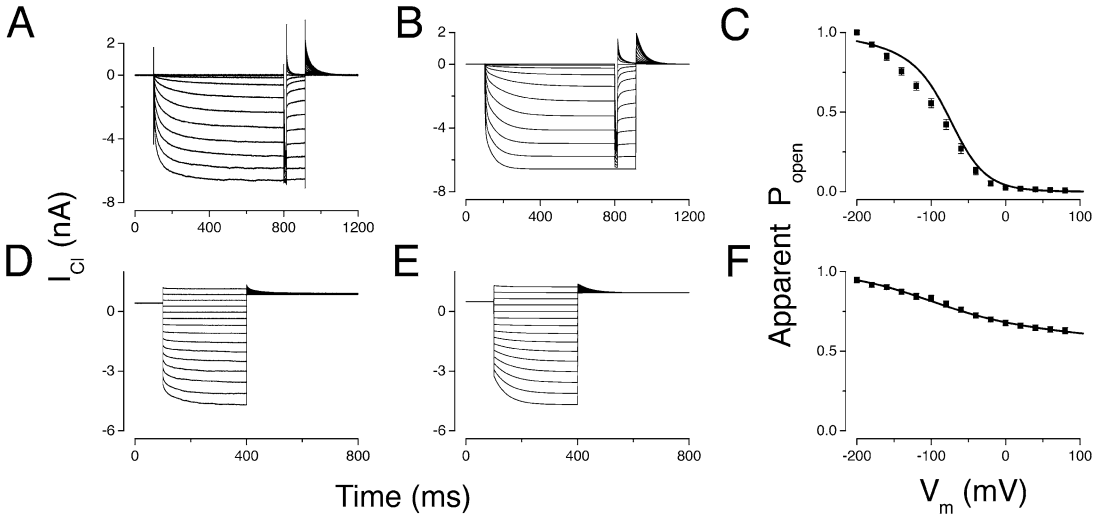

Figure 7. Experiment vs. model. Top trace, raw data obtained from WT mClC-2. Bottom trace, raw data obtained from E213A channels. (A and D) Current traces recorded between +80 and −200 mV. (B and E) Simulated currents between +80 and −200 mV using the model shown in Fig. 6. (C and F) Apparent P_0 experimentally determined (data points) and predicted by the model (continuous lines).

Published December , 2005

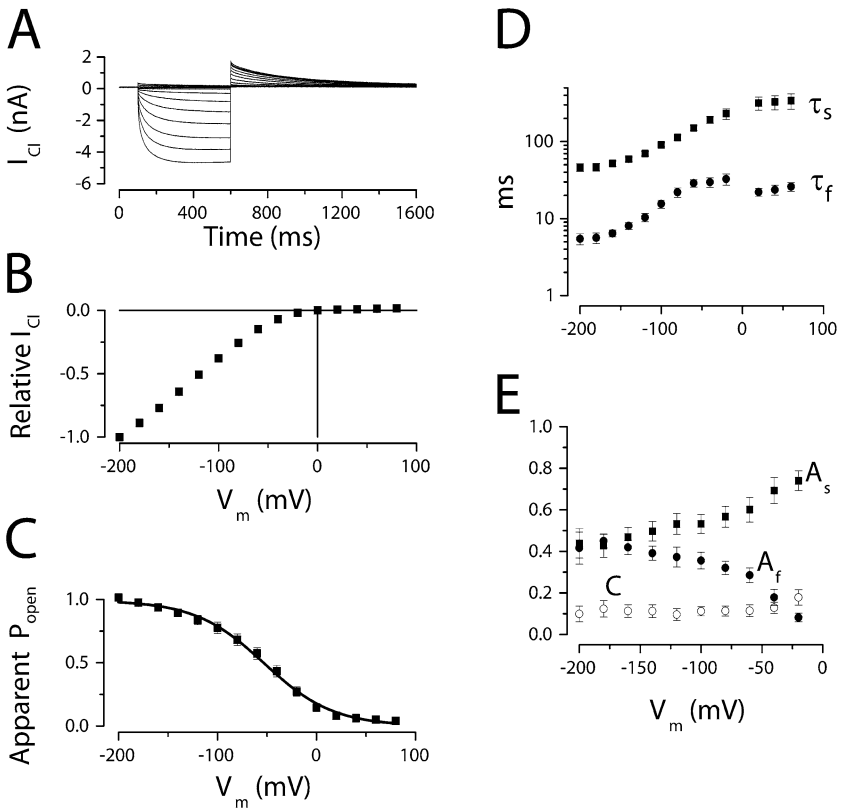

Figure 8. Voltage dependence of C258S mutant channels. (A) Macroscopic currents were recorded using pulses between +80 and −140 mV given in 20-mV increments. Notice that tail currents at +60 mV are slower than those obtained from WT (See Fig. 1). (B) Relative I-V relationship for mutant channels. Current magnitudes were normalized to that obtained at −200 mV and then averaged (n = 6). (C) Apparent P_0 as a function of V_m. Tail currents at +60 mV were used to estimate the P_0 at each V_m (n = 6). Continuous line is a Boltzmann fit. (D) τ_f and τ_s time constants calculated by fitting Eq. 2 to data similar to that shown in A. (E) Relative contributions of A_f and A_s as well as the stationary (C) component that describe the biexponential behavior of C258S channels (n = 6).

with slower kinetics than WT at positive V_m. If the C256 residue is part of the ClC-2 common gate, changing it would not have noticeable effects on closing since the protopore gate closes the pore (this work). Furthermore, this mutation could alter the V_m dependence of the protopore gate (as well as the common gate), thereby altering the closing kinetics. This possibility prompted us to reevaluate the role of residue cysteine C258 in mClC-2 slow gating.

Expression of C258S channels generated noticeable current at 0 mV. Therefore, cells were held at +40 mV. C258S mutant I_{Cl} had onset kinetics quite similar to WT channels (Fig. 8 A; see also Fig. 1 A) at negative V_m. In contrast, closing kinetics at positive V_m were very slow. Although the I-V curve still displayed strong inward rectification (Fig. 8 B), the V_m dependence of apparent P_0 was shifted toward positive voltages compared with WT mClC-2 (Fig. 8 C). Data fit with a Boltzmann function had a half-maximum activating $V_m = -54 \pm 1$ mV and an apparent gating charge of −0.72. τ_f and τ_s for C258S and WT channels show a similar trend at negative V_m (Fig. 8 D), but were slightly faster in C258S channels. However, at positive V_m the time constants continue to increase without showing saturation. Relative contributions of A_f and A_s to the biexponential behavior were also altered. A_f decreased while A_s increased linearly with voltage (Fig. 8 E). Although, this result might be compatible with C258 residue forming part of the common gate, it could also be explained by an altered V_m dependence of both gates.

To evaluate changes in the V_m dependence of the two gates in C258S mutant channels, we determined P_f and P_s as shown in Fig. 2 for WT mClC-2. Fig. 9 displays the resulting P_f and P_s curves. P_f data were fit with a Boltzmann function (Eq. 1) that had values of -24 ± 2 mV and −1.68 for $V_{0.5}$ and z_f, respectively. When compared with WT, the P_f value was shifted by +39 mV in C258S mutant channels. In contrast, the Boltzmann parameters obtained from fitting C258S P_s were $V_{0.5} = -100 \pm 3$ mV and $z_s = -0.41$. C258S P_s was shifted by +35 mV when compared with WT P_s. Thus, C258S altered the V_m dependence of both gates.

To strengthen the observation that mutation C258S disturbs the protopore gate we introduced the same mutation into a background channel lacking the protopore gate (E213A). Since most of E213A channel gating is due to the common gate, the double mutant might also shed light on the role of C258 in common gating. Fig. 10 A shows I_{Cl} obtained from double mutant C258S/E213A channels at different V_m. I_{Cl} were remarkably similar to those of E213A. For example, currents were time independent at $V_m > -50$ mV but at $V_m < -50$ mV, I_{Cl} showed a time dependence similar to that of E213A channels. Furthermore, the I-V curve (Fig. 10 B) and apparent P_0 (Fig. 10 C) were also nearly identical to those of E213A mutant channels (Fig. 4).

Published December , 2005

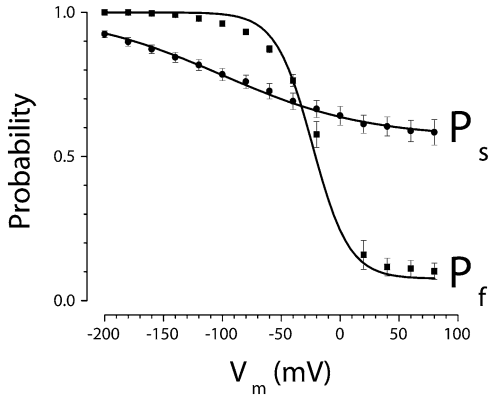

Figure 9. V_m dependence of protopore and common gates in C258S mutant channels. P_f was estimated using the protocol described in Fig. 2. P_s was estimated by dividing apparent P_0 (data shown in Fig. 8 C) by P_F. Continuous lines are fits using Eq. 1 with parameters shown in Table II.

V_m needed to reach half maximum activation was -97 ± 7 mV and the apparent gating charge was -0.35, indicating the lack of the protopore gate. These observations lend support to the idea that mutation C258S has very little effect on the common gate and that the changes produced on channel function are due to alterations in the V_m dependence of the protopore gate. These results are summarized in Table II.

Data obtained from mutant C258S channels show that the protopore gate was strongly influenced by mutating this residue. In Scheme 2, the rate constant β_2 controls the slowest backward transition (C_2 to C_0) of the protopore gate. If C258S slows down the closing of the channels, this might be equivalent to a decrease in this transition rate. Most of the features of the mutant C258S channels can be reproduced by the model (Fig. 6) when the rate constant β_2 at 0 mV was lowered from 10.4 to 1. Fig. 11 compares the model prediction to raw data obtained from a cell expressing C258S mutant channels. The model shows currents with little or no alteration in the "on" kinetics and slow tail currents. In addition, C258S apparent P_0 data was also reproduced (Fig. 11 C).

TABLE II

V_m-dependent Parameters of Protopore and Common Gates from WT and Various Mutant mClC-2 Channels

	$V_{0.5}$ (mV)	Apparent charge	Minimal P_0
Protopore Gate			
WT	-63 ± 1	-1.22	0
C258S	-24 ± 2	-1.68 ± 0.24	0.08 ± 0.03
Common Gate			
WT	-135 ± 3	-0.99	0.55 ± 0.01
C258S	-100 ± 3	-0.41 ± 0.02	0.56 ± 0.01
E213A	-86 ± 3	-0.40 ± 0.01	0.60 ± 0.01
E213AC258S	-97 ± 7	-0.35	0.54 ± 0.01

Parameters were obtained by fitting a Boltzmann equation to V_m-dependent data from each gate.

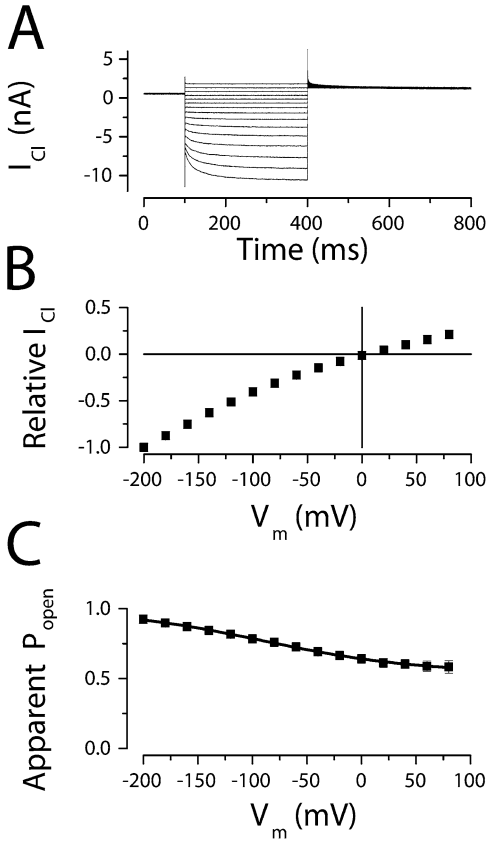

Figure 10. Double mutant C258S/E213A channels. (A) Macroscopic I_{Cl} recorded between +60 and −200 mV ($n = 6$). (B) Relative I-V relationship. (C) Apparent P_0 obtained from tail currents at +60 mV. Continuous line is the fit obtained using Eq. 1.

DISCUSSION

In this work the V_m-dependent gating of mClC-2, a ClC chloride channel cloned from mouse, is described. mClC-2 opening is produced by fast and slow gating processes and the protopore and common gates underlie these processes. However, mClC-2 gating is largely dependent on the protopore gate and much less dependent on the common gate. The V_m dependence of the mClC-2 protopore gate was opposite to those of torpedo ClC-0 and hClC-1 (Lin et al., 1999; Accardi and Pusch, 2000). The V_m dependence of the mClC-2 common gate was similar to that of torpedo ClC-0 but opposite to that of hClC-1. We also show that at positive V_m the protopore gate P_0 decreased sharply to zero while the common gate P_0 did not reach zero. In fact P_s is $\sim$0.6. This implies that the opening rate of individual protopores by a hyperpolarization is mainly controlled by the kinetics of the protopore gate. At very negative V_m, additional channel recruitment to the open state is

Published December , 2005

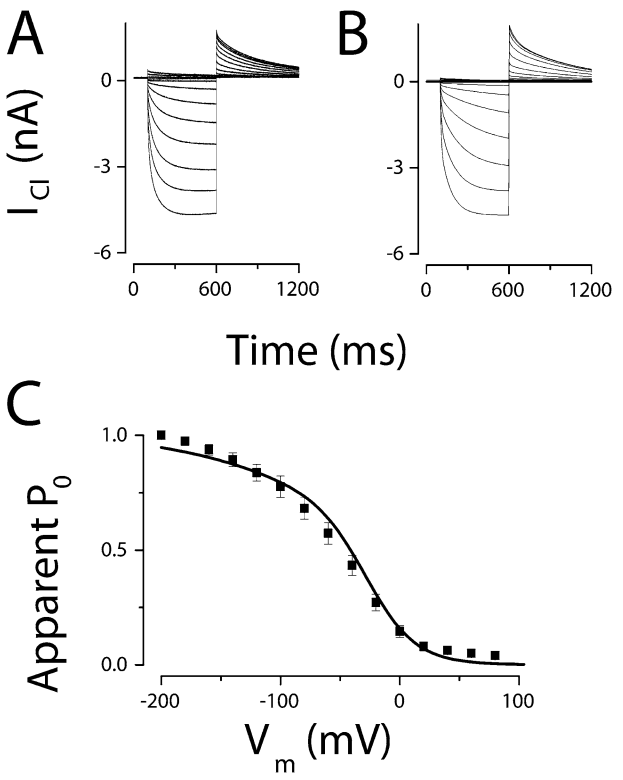

Figure 11. Modeling I_{Cl} from C258S mutant channels. (A and B) I_{Cl} traces between +80 and −140 mV (20-mV increments) were either recorded (A) or reproduced by the model (B). (C) Apparent P_0 as a function of V_m. Probability values shown as filled squares were calculated from tail currents at +60 mV. Continuous line and traces in B were calculated using the model shown in Fig. 6 when $\beta_2 = 1\ s^{-1}$.

achieved by subsequent openings of the common gate. Upon repolarization to positive V_m, the channel closes because the protopore gate P_0 goes to zero.

The recent crystal structure determination of the bacterial protein ClC-ec1 (Dutzler et al., 2003), a ClC homologue with H^+/Cl^- antiporter activity (Accardi and Miller, 2004) allows us to discuss our findings within a structural frame of reference. ClC-ec1 has a glutamic acid (E148) residue facing the pore near the extracellular side, which is conserved in nearly all ClC channels. Mutation analysis revealed that homologue residues in torpedo ClC-0, human ClC-1, and guinea pig ClC-2 channels form the protopore gate (Dutzler et al., 2003; Estevez et al., 2003; Niemeyer et al., 2003). More recently, additional contributions to fast gating resulting from conformational changes in the pore of ClC-0 channel were reported (Accardi and Pusch, 2003). In contrast to protopore gate, the molecular domain(s) responsible for the common gate is more elusive and appears to be more complex (Pusch et al., 1997; Lin et al., 1999; Accardi et al., 2001; Bennetts et al., 2001; Estevez et al., 2004; Zuniga et al., 2004). Mutating cysteine residues 212, 277, and 256 in torpedo ClC-0, human ClC-1, and guinea pig ClC-2 channels, respectively, either completely eliminated or reduced slow inactivation (Lin et al., 1999; Accardi et al., 2001; Zuniga et al., 2004). Moreover, mutating residue H736 located in the CBS2 domain of ClC-0 eliminates slow inactivation (Estevez et al., 2004).

This work shows that mutating the conserved E213 residue abolished the fast gating and a significant fraction of the slow gating in mClC-2. Thus, by analogy with ClC-0 and ClC-1, where mutating an equivalent glutamic acid residue eliminates most of the fast gating, we concluded that the E213 residue forms the protopore gate in mClC-2. However, the protopore gate in mClC-2 has a complex behavior, with at least one closed and two open states. In contrast, a simpler open/closed scheme successfully described the protopore gates of torpedo ClC-0 and hClC-1 channels (Pusch, 2004; Chen, 2005). In the absence of data about Cl^- or pH dependence of mClC-2, Scheme 2 was considered a minimal representation of the conformations that the protopore gate undergoes during channel opening.

The boundaries of fast and slow gating in mClC-2 are less well defined. According to our data, residues affecting only fast or slow gating in torpedo ClC-0 are, in contrast, affecting both processes in mClC-2. Mutating residue C258 in mClC-2 (a similar mutation in torpedo ClC-0 eliminates slow gating; Lin et al., 1999) did not alter greatly the slow gating but produced a rightward shift on the V_m dependence of the protopore gate.

The finding that a three-state model can represent protopore gating kinetics suggests that the returning kinetics of I_{Cl} after a long lasting strong hyperpolarization will follow a quasi monoexponential time course. Under this condition, P_s will return from state C_1 of Scheme 1 and P_f will return from state C_2 of Scheme 2. Returning time constants are slow and quite similar, thus I_{Cl} will be monoexponential. In contrast, the model predicts a faster returning kinetics after a very short hyperpolarization because P_f will return from C_1 (Scheme 2) while P_s remains unchanged. These predictions were experimentally demonstrated (unpublished data), thus lending further support to our model.

It is interesting to note that although a single glutamic acid residue is forming most of the protopore gate in torpedo ClC-0, hClC-1, and mClC-2, the V_m dependence displayed by the mClC-2 protopore gate was opposite to those exhibited by torpedo ClC-0 and hClC-1. Although the origin of this difference is unknown, it has been suggested that in ClC-2 the glutamic acid could be closer to the cytoplasmic side of the membrane where it senses internal but not external $[Cl^-]$ (Niemeyer et al., 2003). Moreover, the protopore gates of torpedo ClC-0, hClC-1, and ClC-2 are modulated differently by $[Cl^-]$. When the ClC-0 has a Cl^- ion bound, it opens by membrane depolarization but in the ab-

Published December , 2005

sence of external Cl^- the opening of the channel is favored by membrane hyperpolarization (Chen, 2005). The apparent P_0 of mClC-2 in contrast, is increased by $[Cl^-]_i$ (Niemeyer et al., 2003; Haug et al., 2003) and hyperpolarizing the membrane voltage increases apparent P_0. It is unknown if mClC-2 opens because the opening of the protopore gate is favored by a hyperpolarization in low $[Cl^-]_e$. In addition, residues other than the glutamic acid might influence fast gating. For example, additional conformational changes in the pore of torpedo ClC-0 (Accardi and Pusch, 2003), which are important for gating, have been documented. Finally, the effects of pH_e on mClC-2 apparent P_0 (Arreola et al., 2002) are different than those observed for ClC-0 and hClC-1. Even though the reason for these differences remains undefined, one or a combination of them may explain why the mClC-2 protopore gate has a V_m dependence and kinetics that are different from those of ClC-0 and ClC-1.

The six-state model, originally proposed to explain ClC-0 function (Miller, 1982; Miller and Richard, 1990), and later used to explain gating of hClC-1, had to be modified in order to explain the function of mClC-2. In particular, the introduction of three states for the protopore gate resulted in a 12-state model. This model was simplified assuming that the transitions between states were independent. With our model we were able to reproduce most of the WT mClC-2 features including kinetics, and V_m dependence of apparent P_0, P_f, and P_s. Furthermore, the model can account for the behavior of E213A and C258S mutant channels. In the case of the E213A mutant channel, the model reproduced I_{Cl} after elimination of P_f.

The slowing down of the closing rate in C258S channels at positive V_m suggests that residue C258 interacted with the protopore gate. A close inspection of the putative location of C258 relative to E213 suggests that these residues are relatively close to each other (we used as a guide the crystal structure of ClC-ecl published by Dutzler et al., 2002) to be coupled. Thus, when the COO^- group of E213 returns to the initial position, its movement could be slowed down by a change in the electrical field near E213. Changes in the local electrical field might be induced by mutating residue C258 into a serine. The original −SH group was changed for a −OH group with opposite orientation. This would explain why residue E213 is necessary for the C258S mutant to alter channel gating. This idea is supported by the double mutant (C258S/E213A) data since the residual gating of E213A and E213A/C258S were indistinguishable. Thus, mutation C258 produced no additional effects on channels lacking E213.

Interestingly, a simple modification of rate constant β_2 that controls the return of the protopore gate from the last state (Fig. 6) was sufficient to explain I_{Cl} resulting from expression of C258S mutant channels. Taken together these observations suggest that residue C258, which in ClC-0 and ClC-1 forms part of the common gate, is coupled to the protopore gate. The idea that ClC gates are not independent has been previously discussed. Pusch's group (Accardi et al., 2001) shows that mutating residue C277 in human ClC-1 altered both fast and slow gating. Furthermore, mutating residue C256 in rat ClC-2 altered both gates (Zuniga et al., 2004). Thus, it seems reasonable to propose that the protopore and common gates are coupled in ClC channels.

In conclusion, we have shown that the underlying gating mechanism of mClC-2 is fully explained by the time and V_m dependence of the protopore and common gates. Furthermore, our data show that a protopore gate that is formed by residue E213 dominates the gating of mClC-2.

The authors thank Dr. Patricia Perez-Cornejo for critical comments and Carmen Y. Hernandez-Carballo for helpful technical assistance.

This work was supported in part by grants R03TW006429-01 (Fogarty International Center, National Institutes of Health [NIH]), 42561 (CONACyT, Mexico), and 1R01 HL080810-01 (NIH). Jose Antonio de Santiago is a Ph.D. student holding a Fellowship Award from CONACyT, Mexico.

David C. Gadsby served as editor.

Submitted: 28 April 2005
Accepted: 27 October 2005

REFERENCES

Accardi, A., and M. Pusch. 2000. Fast and slow gating relaxations in the muscle chloride channel CLC-1. *J. Gen. Physiol.* 116:433–444.

Accardi, A., L. Ferrera, and M. Pusch. 2001. Drastic reduction of the slow gate of human muscle chloride channel (ClC-1) by mutation C277S. *J. Physiol.* 534:745–752.

Accardi, A., and C. Miller. 2004. Secondary active transport mediated by a prokaryotic homologue of ClC Cl^- channels. *Nature.* 427:803–807.

Accardi, A., and M. Pusch. 2003. Conformational changes in the pore of CLC-0. *J. Gen. Physiol.* 122:277–293.

Arreola, J., T. Begenisich, and J.E. Melvin. 2002. Conformation-dependent regulation of inward rectifier chloride channel gating by extracellular protons. *J. Physiol.* 541:103–112.

Bennetts, B., M.L. Roberts, A.H. Bretag, and G.Y. Rychkov. 2001. Temperature dependence of human muscle ClC-1 chloride channel. *J. Physiol.* 535:83–93.

Chen, T.Y., and C. Miller. 1996. Nonequilibrium gating and voltage dependence of the ClC-0 Cl^- channel. *J. Gen. Physiol.* 108:237–250.

Chen, T.Y. 2005. Structures and functions of CLC channels. *Annu. Rev. Physiol.* In press.

Cid, L.P., M.I. Niemeyer, A. Ramirez, and F.V. Sepúlveda. 2000. Splice variants of a ClC-2 chloride channel with differing functional characteristics. *Am. J. Physiol.* 279:C1198–C1210.

de Santiago, J.A., and J. Arreola. 2005. Voltage-dependent gating of ClC-2 chloride channel. *Biophys. J.* 88:615a.

Dutzler, R., E.B. Campbell, M. Cadene, B.T. Chait, and R. MacKin-

non. 2002. X-ray structure of a ClC chloride channel at 3.0 Å reveals the molecular basis of anion selectivity. *Nature.* 415:287–294.

Dutzler, R., E.B. Campbell, and R. MacKinnon. 2003. Gating the selectivity filter in ClC chloride channels. *Science.* 300:108–112.

Estevez, R., B.C. Schroeder, A. Accardi, T.J. Jentsch, and M. Pusch. 2003. Conservation of chloride channel structure revealed by an inhibitor binding site in ClC-1. *Neuron.* 38:47–59.

Estevez, R., M. Pusch, C. Ferrer-Costa, M. Orozco, and T.J. Jentsch. 2004. Functional and structural conservation of CBS domains from CLC channels. *J. Physiol.* 557:363–378.

Fahlke, C., A. Rosenbohm, N. Mitrovic, A.L. George, and R. Rüdel. 1996. Mechanism of voltage-dependent gating in skeletal muscle chloride channels. *Biophys. J.* 71:695–706.

Hamill, O.P., A. Marty, E. Neher, B. Sakmann, and F.J. Sigworth. 1981. Improved patch-clamp techniques for high-resolution current recording from cells and cell-free membrane patches. *Pflüg. Arch. Eur. J. Physiol.* 391:85–100.

Hanke, W., and C. Miller. 1983. Single chloride channels from *Torpedo* electroplax. Activation by protons. *J. Gen. Physiol.* 82:25–42.

Haug, K., M. Warnstedt, A.K. Alekov, T. Sander, A. Ramirez, B. Poser, S. Maljevic, S. Hebeisen, C. Kubisch, J. Rebstock, et al. 2003. Mutations in CLCN2 encoding a voltage-gated chloride channel are associated with idiopathic generalized epilepsies. *Nat. Genet.* 33:527–532.

Jentsch, T.J., V. Stein, F. Weinreich, and A.A. Zdebik. 2002. Molecular structure and physiological function of chloride channels. *Physiol. Rev.* 82:503–568.

Lin, Y.W., C.W. Lin, and T.Y. Chen. 1999. Elimination of the slow gating of ClC-0 chloride channel by a point mutation. *J. Gen. Physiol.* 114:1–12.

Miller, C. 1982. Open-state substructure of single chloride channels from *Torpedo* electroplax. *Philos. Trans. R. Soc. Lond. B. Biol. Sci.* 299:401–411.

Miller, C., and M.M. White. 1984. Dimeric structure of single chloride channels from *Torpedo* electroplax. *Proc. Natl. Acad. Sci. USA.* 81:2772–2775.

Miller, C., and E.A. Richard. 1990. The voltage-dependent chloride channel of *Torpedo* electroplax: intimations of molecular structure from quirks of single-channel function. *In* Chloride Transporters. A. Leefmans and J. Russell, editors. Plenum Publishing Corp., New York. 383–405.

Nehrke, K., J. Arreola, H.V. Nguyen, J. Pilato, L. Richardson, G. Okunade, R. Baggs, G.E. Shull, and J.E. Melvin. 2002. Loss of hyperpolarization-activated Cl^- current in salivary acinar cells from *Clcn2* knockout mice. *J. Biol. Chem.* 277:23604–23611.

Niemeyer, M.I., L.P. Cid, L. Zúñiga, M. Catalán, and F.V. Sepúlveda. 2003. A conserved pore-lining glutamate as a voltage and chloride-dependent gate in the ClC-2 chloride channel. *J. Physiol.* 553:873–879.

Park, K., J. Arreola, T. Begenisich, and J.E. Melvin. 1998. Comparison of voltage-activated Cl^- channels in rat parotid acinar cells with ClC-2 in a mammalian expression system. *J. Membr. Biol.* 163: 87–95.

Pusch, M., U. Ludewig, A. Rehfeldt, and T.J. Jentsch. 1995. Gating of the voltage-dependent chloride channel ClC-0 by the permeant anion. *Nature.* 373:527–531.

Pusch, M., U. Ludewig, and T.J. Jentsch. 1997. Temperature dependence of fast and slow gating relaxations of ClC-0 chloride channels. *J. Gen. Physiol.* 109:105–116.

Pusch, M., A. Accardi, A. Liantonio, L. Ferrera, A. De Luca, D.C. Camerino, and F. Conti. 2001. Mechanism of block of single protopores of the *Torpedo* chloride channel ClC-0 by 2-(*p* chlorophenoxy) butyric acid (CPB). *J. Gen. Physiol.* 118:45–62.

Pusch, M. 2004. Structural insights into chloride and proton-mediated gating of CLC chloride channels. *Biochemistry.* 43:1135–1144.

Richard, E.A., and C. Miller. 1990. Steady-state coupling of ion-channel conformations to a transmembrane ion gradient. *Science.* 247:1208–1210.

Rychkov, G.Y., M. Pusch, D.S.J. Astill, M.L. Roberts, T.J. Jentsch, and A.H. Bretag. 1996. Concentration and pH dependence of skeletal muscle chloride channel ClC-1. *J. Physiol.* 497:423–435.

Thiemann, A., S. Gründer, M. Pusch, and T.J. Jentsch. 1992. A chloride channel widely expressed in epithelial and non-epithelial cells. *Nature.* 356:57–60.

Weinreich, F., and T.J. Jentsch. 2001. Pores formed by single subunits in mixed dimers of different CLC chloride channels. *J. Biol. Chem.* 276:2347–2353.

Zuniga, L., M.I. Niemeyer, D. Varela, M. Catalan, L.P. Cid, and F.V. Sepulveda. 2004. The voltage-dependent ClC-2 chloride channel has dual gating mechanism. *J. Physiol.* 555:671–682.